Influence of Ca substitution by Mg on the $Ca_3Co_4O_9$ performances

G. Constantinescu[1], Sh. Rasekh[1], M. A. Torres[2], J. C. Diez[1], M. A. Madre[1], A. Sotelo[1]

[1]ICMA (UZ-CSIC), Dpto. de Ciencia y Tecnología de Materiales y Fluidos, C/María de Luna 3, E-50018, Zaragoza (Spain)

[2]Universidad de Zaragoza, Dpto. de Ingeniería de Diseño y Fabricación, C/María de Luna 3, E-50018, Zaragoza (Spain)

Abstract

$Ca_{3-x}Mg_xCo_4O_9$ polycrystalline thermoelectric ceramics with small amounts of Mg have been synthesized by the classical solid state method. Microstructural characterizations have shown that all the Mg has been incorporated into the $Ca_3Co_4O_9$ structure and no Mg-based secondary phases have been identified. Apparent density measurements have shown that samples do not modify their density until 0.05 Mg content, decreasing for higher contents. Electrical resistivity decreases and Seebeck coefficient slightly raises when Mg content increases until 0.05 Mg addition. The improvement in both parameters leads to higher power factor values than the usually obtained in samples prepared by the conventional solid state routes and close to those obtained in textured materials.

Keywords: Doping; Sintering; Cobaltites; Electrical properties; Thermopower.

Resumen

Se han preparado cerámicas termoeléctricas policristalinas de $Ca_{3-x}Mg_xCo_4O_9$, con pequeñas cantidades de Mg, utilizando el método clásico de estado sólido. La caracterización microestructural ha mostrado que el Mg se ha incorporado en la estructura del $Ca_3Co_4O_9$ y que no se han formado fases secundarias con el Mg. Las medidas de densidad aparente han mostrado que las muestras prácticamente poseen la misma densidad hasta un contenido de 0.05 Mg, disminuyendo para contenidos mayores. La resistividad eléctrica disminuye y el coeficiente Seebeck aumenta cuando el contenido de Mg se incremento hasta valores de 0.05. La mejora de ambos parámetros conduce a valores del factor de potencia mayores que los obtenidos en muestras preparadas por la vía convencional de estado sólido, alcanzando valores próximos a los que se encuentran en materiales texturados.

Keywords: Dopado; Sinterizado; Cobaltitas; Propiedades eléctricas; Poder termoeléctrico.

Corresponding author: G. Constantinescu

e-mail: gconstan@unizar.es

Address: Dept. Ciencia de Materiales; C/Mª de Luna, 3; 50018-Zaragoza; Spain

Tel: +34 976762617

Fax: +34 976761957

1. Introduction

Thermoelectric (TE) materials are able to transform a temperature gradient to electrical power directly, without moving parts, due to the Seebeck effect. This intrinsic property has focused attention on these materials as they can be applied in waste heat recovery devices [1] or solar thermoelectric generators [2]. Furthermore, they can also be used as heating/refrigeration devices due to the Peltier effect [3]. The conversion efficiency of these materials is usually quantified by the dimensionless figure-of-merit ZT, $TS^2/\rho\kappa$ (in which the electrical part S^2/ρ is also called power factor, PF), where S is the Seebeck coefficient (or thermopower), ρ the electrical resistivity, κ the thermal conductivity, and T is the absolute temperature [4].

Taking into account the above expression for the figure-of-merit, high performance materials should possess a large Seebeck coefficient together with low electrical resistivity and thermal conductivity. The low electrical resistivity is necessary to minimize Joule heating, while the low thermal conductivity helps to maintain a large temperature gradient between the hot and cold sides in the thermoelectric device, increasing the developed voltage.

Nowadays the industrially applied TE devices are based on intermetallic materials, such as Bi_2Te_3 or $CoSb_3$, with high ZT values at relatively low temperatures. However, they cannot be applied in devices working at high temperatures under air due to their degradation and/or heavy metals evaporation. As a consequence, their ability to harvest energy from waste heat sources is strongly limited by their working temperatures. These limitations in temperature were overcome in 1997 by the discovery of relatively high thermoelectrical properties in a Co-based oxide ceramic, the $Na_2Co_2O_4$ [5].

From its discovery, many works have been performed on different cobaltite ceramic families as promising thermoelectric materials for high temperature applications, as the Bi-M-Co-O-based (M: alkaline earth) materials [6-8]. At the moment, research is mainly focused on Bi-free ceramic materials with high thermoelectric performances and higher thermal stability, such as $Ca_3Co_4O_9$, with promising thermoelectric properties [9,10].

Crystallographic studies performed on those Co-based materials have demonstrated that they present monoclinic crystal structure which is, in turn, composed of two different layers. These layers show an alternate stacking of a common conductive CdI_2-type hexagonal CoO_2 layer with a two-dimensional triangular lattice, and a block layer composed of insulating rock-salt-type (RS) layers. The two sublattices (RS block and CdI_2-type CoO_2 layer) possess common a- and c-axis lattice parameters and β angles, but different b-axis length, causing a misfit along the b-direction [11,12]. Furthermore, the high crystallographic anisotropy of these materials is reflected in their preferential growth habit along the ab plane (coincidental with the conducting plane), which leads to the formation of plate-like grains during the sintering process. This preferential growth habit can be exploited to preferentially align the grains using physical, mechanical and/or chemical processes. Such processes allow the alignment of the conducting planes producing macroscopic properties comparable to the obtained on single crystals, by decreasing electrical resistivity. Numerous methods have been reported to be efficient in producing well aligned bulk materials, in these or in similar anisotropic systems, such as hot uniaxial pressing [13], spark plasma sintering (SPS) [14], microwave texturing [15], laser floating zone melting (LFZ) [16,17], electrically asisted laser

floating zone (EALFZ) [18,19], templated grain growth (TGG) [20], *etc*. The main advantage of these techniques is the production of materials with very low electrical resistivity values due to the preferential alignment of conducting planes with the current flow direction. On the other hand, they possess some drawbacks, as the high price of the spark plasma device and the relatively long processing time of the hot uniaxial pressing or the TGG. In the case of the processes involving samples melting, it has been reported that the electrical properties are strongly dependent on the growth speed [15,21-23]. All these drawbacks have, as a consequence, an important influence on the industrial interest for the materials processed by these techniques.

It has also been reported that the Seebeck coefficient values are governed by the incommensurability ratio and/or the charge of the RS block layer between the CoO_2 ones [24]. This effect provides the basis for the modification of thermoelectric properties of a given material via chemical substitutions, as Sb^{3+} for Ca^{2+} in $Ca_3Co_4O_9$ [25], or Pb^{2+} for Bi^{3+} in $Bi_2Sr_2Co_{1.8}O_x$ or $Bi_2Ca_2Co_{1.7}O_x$ [26-28]. Other improvements can be produced by metallic Ag additions where an increase on the materials performances is produced by raising the electrical connectivity between the grains [29,30], or substituting $Co^{3+/4+}$ by other transition metal, as Cu^{2+} or Cr^{3+} in $Ca_3Co_4O_9$ [31,32].

The aim of this work is to study the effect of small amounts of Mg^{2+} for Ca^{2+} isovalent substitution on the microstructure and high temperature thermoelectric properties of $Ca_{3-x}Mg_xCo_4O_y$ prepared by the simple classical solid state synthesis route. The structural and microstructural modifications produced by the Mg addition will be related with the changes on the thermoelectric performances.

2. Experimental

$Ca_{3-x}Mg_xCo_4O_9$ polycrystalline ceramic materials, with x = 0.00, 0.01, 0.03, 0.05, and 0.07, were prepared by the conventional solid state route using $CaCO_3$ (Panreac, 98 + %), MgO (Panreac, 98 + %), and Co_2O_3 (Aldrich, 98 + %) commercial powders as starting materials. They were weighed in the appropriate proportions, well mixed and ball milled for 30 minutes at 300 rpm, in acetone media, in an agate ball mill. The obtained slurry has been heated under infrared radiation during about 30 minutes to produce the acetone evaporation, leaving a homogeneous powder mixture. This dry mixture was then manually milled in order to avoid the presence of agglomerates in the next steps. After milling, the homogeneous mixture of fine powders was thermally treated twice at 750 and 800ºC for 12h under air, with an intermediate manual milling in order to assure the total decomposition of calcium carbonate, as reported previously [10], which improves the mixture reactivity during the sintering processes. After the thermal treatments, the powders were uniaxially pressed at 400 MPa for 1 minute in order to obtain green ceramic parallelepipeds (~ 3 mm x 2.5 mm x 14 mm), with an adequate size for their thermoelectric characterization. These green ceramics were subsequently sintered at 910 ºC for 24 h, typical temperatures used in this kind of compounds [31].

Powder X-ray diffraction (XRD) patterns have been systematically recorded in order to identify the different phases in the thermoelectric materials after sintering procedure. Data have been collected at room temperature, with 2θ ranging between 5 and 60 degrees, using a Rigaku D/max-B X-ray powder diffractometer working with Cu Kα radiation. Apparent density measurements

have been performed by measuring the dimensions and weighting the samples for three times to avoid errors. At least four sintered samples of each composition were used to obtain the mean apparent density values and compared with the theoretical density (4.677 g/cm^3) [33].

Microstructural observations were performed on the surface of samples, using a Field Emission Scanning Electron Microscope (FESEM, Carl Zeiss Merlin) fitted with an energy dispersive spectrometry (EDS) analyzer. Several micrographs of the samples have been used to analyze the different phases composition and their distribution. Electrical resistivity and Seebeck coefficient were simultaneously determined by the standard dc four-probe technique in a LSR-3 measurement system (Linseis GmbH), in the steady state mode and at temperatures ranging from 50 to 800 ºC under He atmosphere. From the resistivity values, the activation energy and the relative carrier concentration for each sample have been estimated. Moreover, with the electrical resistivity and thermopower data, the power factor has been calculated in order to determine the samples performances. These properties have been compared with the results obtained in the undoped samples and with those reported in the literature at low temperatures (~ 50 ºC), where oxygen diffusion is negligible, to avoid the influence of the atmosphere on the compared values.

3. Results and discussion

Powder XRD patterns for the different $Ca_{3-x}Mg_xCo_4O_9$ samples are displayed in Fig. 1 (from 5 to 40º for clarity). From these data, it is clear that all the samples have very similar diffraction patterns. In these plots, the peak marked by # in Fig. 1e belongs to the (111) diffraction plane of Si, used as internal reference. In

Fig. 1a, corresponding to the undoped samples, major peaks have been associated with the thermoelectric $Ca_3Co_4O_9$ phase, indicated by its reflection planes, in agreement with previously reported data [34]. When Mg is added to the samples, the peaks corresponding to the $Ca_3Co_2O_6$ secondary phase (shown by * in Fig 1e) [34] increase their intensity, indicating the raise of this phase contents. On the other hand, careful observation of these diagrams shows that there is no evidence of other secondary phases, especially Mg-containing ones, which is a clear indication that Mg has entered into the $Ca_3Co_4O_9$ and/or $Ca_3Co_2O_6$ phases.

Fig. 2 shows SEM micrographs performed on the surface of some representative samples corresponding to the 0.01 (a) and 0.05 (b) Mg substituted ones. In the figure, it can be clearly seen that all samples are composed by randomly oriented plate-like grains with similar sizes. When observing the samples in more detail, it has been found that major phase is the thermoelectric $Ca_3Co_4O_9$ one (grey contrast, #1) which can be observed as well defined plate-like grains. $Ca_3Co_2O_6$ secondary phase (#2) can be also seen in all samples as a very slightly darker grey contrast, easily distinguishable by their shape (as illustrated with Fig. 2c), but in a much lower proportion than the main phase. These observations are in agreement with the above discussed XRD data. On the other hand, EDS analysis has shown that Mg incorporation is produced in the $Ca_3Co_4O_9$ crystal structure by substituting Ca (see Table I). Other interesting feature which can be observed in Fig. 2 is that the samples are not fully dense, presenting porosity which can be observed in the micrographs as black contrast. This is due to the relatively low temperature stability of the thermoelectric phase (maximum stability temperature ~ 926 ºC),

compared with the minimum temperature to produce a liquid phase (~ 1350 ºC) [34]. The great difference between both temperatures leads to a very slow densification process at the sintering temperatures (~ 910 ºC), explaining the porosity obtained in these samples.

When observing the samples at higher magnification, some small differences can be detected in those with the highest Mg addition (0.07 Mg). This is illustrated in Fig. 3 where a high magnification micrograph performed on the surface of this sample is presented. As it is evident in the micrograph, a new type of grains is appearing (indicated by #3). These grains possess a shape which is different to the observed for the phases #1 and #2, and they can be seen as more or less triangular grains. Furthermore, EDS analysis has shown that their composition corresponds to a Mg-rich and Ca-deficient phase (Table I). In any case, this phase is in a very small proportion which explains the reason why it has not been detected with the XRD technique.

In order to evaluate the samples density, apparent density measurements have been performed on at least 4 samples for each composition. They were measured and weighed for three times to minimize the errors. The calculated apparent densities, together with their standard error, are represented in Fig. 4 *vs.* Mg contents. In the figure, it is clear that samples density is maintained approximately constant until 0.05 Mg-doping, and significantly decreasing for the 0.07 Mg containing sample. Moreover, the standard error is increased for these samples, indicating that the values dispersion is higher than for the other samples. These differences on the apparent density imply that they are ~ 75% of the theoretical one for all the samples except for the 0.07 Mg-doped one which is decreased to ~ 70%. These density variations for the low doped

samples are small enough to assume that density values practically have no effect on the electrical behaviour of the samples except in the case of the highest Mg-doped samples.

Fig. 5 shows the variation of the Seebeck coefficient with the temperature, as a function of the Mg doping. In the plot, it can be clearly seen that the sign of the thermopower is positive for the entire measured temperature range, which confirms a conduction mechanism mainly governed by holes. The values of the Seebeck coefficient increase with temperature, with similar behaviour for all the samples. The main differences between samples are observed at high temperatures, as the room temperature values are approximately the same for all samples, independently of Mg content. This measured value (around 135 μV/K) is slightly higher than those reported elsewhere for Mg-doped samples (~ 125 μV/K) at 200 ºC [35]. At high temperatures, undoped samples and 0.01Mg ones show the same values in all the measured temperature range due to the very small amount of Mg, which is not enough to modify Seebeck coefficient values. The effect of Mg can be seen in samples with 0.03 and 0.05 Mg which slightly increase the Seebeck values at high temperatures, compared with the lower doped samples. This behaviour is in agreement with previously published results which show that the decrease on the rock salt layer size promotes higher Seebeck values [24]. Finally, for the highest Mg content samples the Seebeck coefficient decreases, due to the higher content of $Ca_3Co_2O_6$ secondary phase and the formation of isolated $Ca_{2.5}Mg_{0.5}Co_4O_9$ grains which probably do not contribute to the measured Seebeck coefficient values. The maximum measured Seebeck coefficient value (~ 210 μV/K) at 800 ºC corresponds to the 0.03 Mg-doped samples higher than the obtained for the

undoped ones. Moreover, S values at 625 ºC (~ 195 μV/K) are also higher than the best values obtained for undoped $Ca_3Co_4O_9$ samples sintered and textured by spark plasma sintering (170-175 μV/K) at the same temperature [36]. The relatively similar values obtained for the undoped and the Mg-doped samples indicate that Mg doping does not affect, in a great extent, the $Ca_3Co_4O_9$ conduction band [32].

The temperature dependence of electrical resistivity, as a function of the Mg content, is shown in Fig. 6. As can be clearly seen, the ρ (T) curves show a decrease of the measured resistivity from 0.00 to 0.05 Mg substitution. Higher Mg contents increases resistivity, compared with the other Mg-doped samples. These curves reflect a slope change at about 400 ºC, from semiconducting-like ($d\rho/dT \leq 0$) to metallic-like ($d\rho/dT \geq 0$) one. All the Mg-substituted samples present lower resistivity values than the undoped ones. The lowest measured room temperature resistivity values (~ 15 mΩ.cm for the 0.05 Mg-substituted samples) is around the best values obtained for $Ca_3Co_4O_9$ samples sintered and textured by spark plasma sintering (15-18 mΩ.cm) [36] and about 30 % lower than the undoped samples prepared in this work.

In order to explain the resistivity behaviour of these samples, it should be considered that the temperature dependence of the electrical conductivity, in the semiconductor behaviour zone, can be described as:

$$\sigma.T \propto \exp (E/k_B.T)$$

where E, k_B, and T are the activation energy, Boltzmann constant, and absolute temperature, respectively. The activation energy values were obtained from the log (σT) *versus* 1/T plot as the curve fit slope in the different samples below T*, as illustrated in Fig. 7. T* is defined as the temperature where the behaviour of

the samples changes from semiconducting-like to metallic-like one. The calculated values have been found to be around 40 meV in all cases, confirming that Mg addition does not modify appreciably the $Ca_3Co_4O_9$ conduction band. On the other hand, two differences between doped and undoped samples can be pointed out from this graph. Firstly, Mg addition shift the T^* to lower temperature values, indicating a change to metallic-like behaviour at lower temperature due to the fact that Mg doping increases the metallic characteristics of the compound (see T_1^* and T_2^* in Fig. 7, corresponding to the undoped and Mg-doped samples, respectively). Secondly, the carrier concentration is increased when Mg is added to the samples, as the log (σT) *versus* 1000/T curves appear at higher values, until 0.05 Mg addition, decreasing for higher Mg contents. Under the assumption that these changes in conductivity are mainly due to variations on the hole concentration, the relative increase, compared with the undoped samples, has been estimated and displayed in Fig. 8. From this figure, it is clear that the raise in Mg contents increase the hole carrier concentration until a maximum of around 45 % for the samples with 0.05 Mg substitution. Further Mg addition decreases the conductivity due to an increase of defects in the crystal structure reflected in lower carrier mobility, avoiding the effect of a higher carrier concentration.

In order to evaluate the thermoelectric performances of these materials, the power factor has been calculated. The temperature dependence of the power factor, calculated from the data represented in Figs. 5 and 6, is plotted in Fig. 9. When considering PF values at around 50 ºC (~ room temperature), it can be clearly seen that all the Mg-doped samples possess higher PF values than the undoped ones. The maximum increase is obtained for the 0.05 Mg-doped

samples (~ 45 % higher than the undoped ones). The highest PF value obtained at 800 ºC (around 0.28 mW/K^2.m) for the 0.05 Mg-doped samples is relatively close to the values obtained in samples sintered and textured by spark plasma sintering (~ 0.32 mW/K^2.m) [36]. This 0.28 mW/K^2.m maximum value is a very important result when taking into account that the Mg substituted samples prepared for this work possess randomly oriented grains and, as a consequence, they should show much lower thermoelectric performances than the textured materials.

4. Conclusions

This paper demonstrates that Mg can substitute Ca in $Ca_{3-x}Mg_xCo_4O_9$ in small proportions ($x \leq 0.05$) without appreciably modifying the crystal structure and improving the thermoelectric properties. Further Mg addition slightly diminishes thermoelectric performances. The optimal Mg for Ca substitution has been determined using the values of the power factor at 50 and 800 ºC, which is maximum for the 0.05 Mg-doped samples with values around 0.13 and 0.28 mW/K^2.m, respectively, which are about 45 and 55 % higher than the obtained for the undoped samples at these temperatures. Moreover, the value at 800 ºC is very close to the obtained in textured samples produced by spark plasma sintering under pressure. This value is very important for samples which possess randomly oriented grains.

Acknowledgements

The authors wish to thank the Gobierno de Aragón (Research Groups T12 and T87) for financial support. The technical contributions of C. Estepa, and C.

Gallego are also acknowledged. Sh. Rasekh also acknowledges a JAE-PreDoc 2010 grant from CSIC.

References

[1] Mahan G., Sales B.; Sharp J. (1997): Thermoelectric materials: New approaches to an old problem, *Phys. Today,* 50: 42-47.

[2] Naito H.; Kohsaka Y.; Cooke D.; Arashi H. (1996): Development of a solar receiver for a high-efficicency thermionic/thermoelectric conversion system, *Solar Energy,* 58 (4-6): 191–195.

[3] Kim C. M.; Hwang Y. J.; Ryu Y. H. (2002): Air conditioner for individual cooling/heating, US Patent US6393842. May,

[4] Rowe D.M. (2006): *Thermoelectrics Handbook: Macro to Nano,* 1st edn, CRC Press, Boca Raton, FL, pp. 1-3–1-7.

[5] Terasaki I.; Sasago Y.; Uchinokura K. (1997): Large thermoelectric power in $NaCo_2O_4$ single crystals, *Phys. Rev. B*, 56: 12685-12687.

[6] Madre M. A.; Rasekh Sh.; Diez J. C.; Sotelo A. (2010): New solution method to produce high performance thermoelectric ceramics: A case study of Bi-Sr-Co-O, *Mater. Lett*., 64: 2566-2568.

[7] Sotelo A.; Rasekh Sh.; Madre M. A.; Guilmeau E.; Marinel S.; Diez J. C. (2011): Solution-based synthesis routes to thermoelectric $Bi_2Ca_2Co_{1.7}O_x$, *J. Eur. Ceram. Soc.,* 31: 1763-1769.

[8] Constantinescu G.; Rasekh Sh.; Torres M. A.; Madre M. A.; Diez J. C.; Sotelo A. (2013): Enhancement of the high-temperature thermoelectric performance of $Bi_2Ba_2Co_2O_x$ ceramics, *Scripta Mater.,* 68: 75-78.

[9] Funahashi R.; Matsubara I.; Ikuta H.; Takeuchi T.; Mizutani U., Sodeoka S. (2000): An oxide single crystal with high thermoelectric performance in air, *Jpn. J. Appl. Phys,.* 39: L1127-1129.

[10] Sotelo A.;Constantinescu G.; Rasekh Sh.; Torres M. A.; Diez J. C.; Madre M. A. (2012): Improvement of thermoelectric properties of $Ca_3Co_4O_9$ using soft chemistry synthetic methods, *J. Eur. Ceram. Soc*., 32: 2415-2422.

[11] Maignan A.; Hébert S.; Hervieu M.; Michel C.; Pelloquin D.; Khomskii D. (2003): Magnetoresistance and magnetothermopower properties of Bi/Ca/Co/O and Bi(Pb)/Ca/Co/O misfit layer cobaltites, *J. Phys.: Condens. Matter.,* 15: 2711-2723.

[12] Itahara H.; Xia C.; Sugiyama J.; Tani T. (2004): Fabrication of textured thermoelectric layered cobaltites with various rock salt-type layers by using β-$Co(OH)_2$ platelets as reactive templates, *J. Mater. Chem,.* 14: 61-66.

[13] Kenfaui D.; Chateigner D.; Gomina M.; Noudem J. G. (2011): Anisotropy of the mechanical and thermoelectric properties of hot-pressed single-layer and multilayer thick $Ca_3Co_4O_9$ ceramics, *Int. J. Appl. Ceram. Technol.* 8: 214-226.

[14] Liu Y.; Lin Y.; Nan C.-W.; Shen Z. (2005): Preparation of $Ca_3Co_4O_9$ and improvement of its thermoelectric properties by spark plasma sintering, *J. Am. Ceram. Soc.* 88: 1337-1340.

[15] Marinel S.; Bourgault D.; Belmont O.; Sotelo A.; Desgardin G. (1999): Microstructure and transport properties of YBCO zone melted samples processed in a microwave cavity and infra-red furnace, *Physica C,* 315: 205-214

[16] Sotelo A.; Guilmeau E.; Madre M. A.; Marinel S.; Diez J. C.; Prevel M. (2007): Fabrication and properties of textured Bi-based cobaltite thermoelectric rods by zone melting, *J. Eur. Ceram. Soc*., 27: 3697-3700.

[17] Diez J. C.; Rasekh Sh.; Madre M. A.; Guilmeau E.; Marinel S.; Sotelo A. (2010): Improved thermoelectric properties of Bi-M-Co-O (M = Sr, Ca) misfit

compounds by laser directional solidification, *J. Electron. Mater*., 39: 1601-1605.

[18] Ferreira N. M.; Rasekh Sh.; Fernandes A. J. S.; Costa F. M.; Madre M. A.; Diez J. C.; Sotelo A. (2012): Electrical polarization effect on $Bi_2Ca_2Co_{1.7}O_x$ thermoelectrics grown by laser floating zone, *Microsc. Microanal*., 18: 93-94.

[19] Ferreira N. M.; Rasekh Sh.; Costa F. M.; Madre M. A.; Sotelo A.; Diez J. C.; Torres M. A. (2012) New method to improve the grain alignment and performance of thermoelectric ceramics*, Mater. Lett*., 83: 144-147.

[20] Seabaugh M. M.; Kerscht I. H.; Messing C. L. (1997): Texture development by templated grain growth in liquid-phase-sintered alpha-alumina, *J. Am. Ceram. Soc*., 80: 1181-1188.

[21] Sotelo A.; Guilmeau E.; Madre M. A.; Marinel S.; Lemmonier S.; Diez J. C. (2008): $Bi_2Ca_2Co_{1.7}O_x$ thermoelectric ceramics textured by laser floating zone method, *Bol. Soc. Esp. Ceram. V*., 47: 225-228.

[22] Diez J. C.; Guilmeau E.; Madre M. A.; Marinel S.; Lemmonier S.;Sotelo A. (2009): Improvement of $Bi_2Sr_2Co_{1.8}O_x$ thermoelectric properties by laser floating zone texturing, *Solid State Ionics*, 180: 827-830.

[23] Rasekh Sh.; Constantinescu G.; Torres M. A.; Madre M. A.; Diez J. C.; Sotelo A. (2012): Growth rate effect on microstructure and thermoelectric properties of melt grown $Bi_2Ba_2Co_2O_x$ textured ceramics, *Adv. Appl. Ceram*., 111: 490-494.

[24] Maignan A.; Pelloquin D.; Hébert S.; Klein Y.; Hervieu M. (2006): Thermoelectric power in misfit cobaltites ceramics: Optimization by chemical substitutions, *Bol. Soc. Esp. Ceram. V.*, 45: 122-125.

[25] Demirel S.; Aksan M. A.; Altin S. (2012): Low temperature electrical and thermal transport properties of the $Ca_{3-x}Sb_xCo_4O_9$ system, *J. Mater. Sci.: Mater. Electron*., 23: 2251-2256.

[26] Sotelo A.; Rasekh Sh.; Guilmeau E.; Madre M. A.; Torres M. A.; Marinel S.; Diez J. C. (2011): Improved thermoelectric properties in directionally grown $Bi_2Sr_2Co_{1.8}O_y$ ceramics by Pb for Bi substitution, *Mater. Res. Bull*., 46: 2537-2542.

[27] Sotelo A.; Guilmeau E.; Rasekh Sh.; Madre M. A.; Marinel S., Diez J. C (2010), Enhancement of the thermoelectric properties of directionally grown Bi-Ca-Co-O through Pb for Bi substitution, *J. Eur. Ceram. Soc*., 30: 1815-1820.

[28] Rasekh Sh.; Madre M. A.; Diez J. C.; Guilmeau E.; Marinel S.; Sotelo A. (2010): Effect of Pb substitution on the thermoelectrical properties of textured $Bi_2Ca_2Co_{1.7}O_y$ ceramics prepared by a polymer solution method, *Bol. Soc. Esp. Ceram. V*., 49: 371-376.

[29] Sotelo A.; Torres M. A.; Constantinescu G.; Rasekh Sh.; Diez J. C.; Madre M. A. (2012): Effect of Ag addition on the mechanical and thermoelectric performances of annealed $Bi_2Sr_2Co_{1.8}O_x$ textured ceramics, *J. Eur. Ceram. Soc*., 32: 3745-3751.

[30] Sotelo A.;Rasekh Sh.; Constantinescu G.; Torres M. A.; Madre M. A.; Diez J. C. (2013): Improvement of textured $Bi_{1.6}Pb_{0.4}Sr_2Co_{1.8}O_x$ thermoelectric performances by metallic Ag additions, *Ceram. Int*., 39: 1597-1602.

[31] Rasekh Sh.; Torres M. A.; Constantinescu G.; Madre M. A.; Diez J. C.; Sotelo A. (2013): Effect of Cu by Co substitution on $Ca_3Co_4O_9$ thermoelectric ceramics. *J. Mater. Sci.: Mater. Electron*., 24: 2309-2314

[32] Diez J. C.; Torres M. A.; Rasekh Sh.; Constantinescu. G.; Madre M. A.; Sotelo A. (2013). Enhancement of $Ca_3Co_4O_9$ thermoelectric properties by Cr for Co substitution. *Ceram. Int.*, 39: 6051-6056

[33] Liou Y. C.; Tsai W. C.; Lin W. Y.; Lee U. R. (2008): Synthesis of $Ca_3Co_4O_9$ and $CuAlO_2$ ceramics of the thermoelectric application using a reaction-sintering process, *J. Aust. Ceram. Soc.*, 44: 17–22.

[34] Woermann E.; Muan A. (1970): Phase equilibria in the system CaO-cobalt oxide in air, *J. Inorg. Nucl. Chem*., 32: 1455-1459.

[35] Matsubara I.; Funahashi R.; Shikano M. (2002): Effects of cation substitution on the thermoelectric properties in Ca-Co-O*. Mat. Res. Soc. Symp. Proc.*, 691: 393-398.

[36] Kenfaui D.; Bonnefont G.; Chateigner D.; Fantozzi G.; Gomina M.; Noudem J. G (2010): $Ca_3Co_4O_9$ ceramics consolidated by SPS process: Optimisation of mechanical and thermoelectric properties, *Mater. Res. Bull*., 45: 1240-1249.

Figure captions:

Figure 1. Powder X-ray diffraction patterns obtained for the $Ca_{3-x}Mg_xCo_4O_9$ samples; x = 0.00 (a); 0.01 (b); 0.03 (c); 0.05 (d); and 0.07 (e). The diffraction planes indicate the $Ca_3Co_4O_9$ phase and those marked by a * the $Ca_3Co_2O_6$ one. The # symbol denotes the (111) plane of Si used as internal reference.

Figure 2. Surface SEM micrographs of $Ca_{3-x}Mg_xCo_4O_9$ samples for x = 0.01 (a); and 0.05 (b) showing the randomly oriented plate-like grains. The two different contrasts have been associated with: 1) $Ca_3Co_4O_9$; and 2) $Ca_3Co_2O_6$ phases. Close view (c) of one Mg-substituted sample showing with an arrow the $Ca_3Co_2O_6$ phase.

Figure 3. High magnification surface SEM micrograph of $Ca_{2.93}Mg_{0.07}Co_4O_9$ sample showing the new $Ca_{2.5}Mg_{0.5}Co_4O_9$ phase as approximately triangular grains indicated by the arrow.

Figure 4. Apparent density values, together with their standard error, as a function of the Mg doping.

Figure 5. Temperature dependence of the Seebeck coefficient as a function of Mg content in $Ca_{3-x}Mg_xCo_4O_9$ samples, for x = 0.00 (●); 0.01 (▲); 0.03 (▼); 0.05 (■); and 0.07 (◆).

Figure 6. Temperature dependence of the electrical resistivity, as a function of Mg content in $Ca_{3-x}Mg_xCo_4O_9$ samples, for x = 0.00 (●); 0.01 (▲); 0.03 (▼); 0.05 (■); and 0.07 (◆).

Figure 7. Log (σT) *versus* 1000/T plot for all the $Ca_{3-x}Mg_xCo_4O_9$ samples, for x = 0.00 (●); 0.01 (▲); 0.03 (▼); 0.05 (■); and 0.07 (◆). The slopes of the fittings are nearly the same in all cases, below T*. T_1* and T_2* indicate the metallic-to-semiconducting transition temperature for the undoped and Mg-doped samples, respectively.

Figure 8. Relative variation of carrier concentration, compared with the undoped samples, as a function of Mg content of the samples.

Figure 9. Temperature dependence of the power factor as a function of Mg content in $Ca_{3-x}Mg_xCo_4O_9$ samples, for x = 0.00 (●); 0.01 (▲); 0.03 (▼); 0.05 (■); and 0.07 (◆).

Figure 1

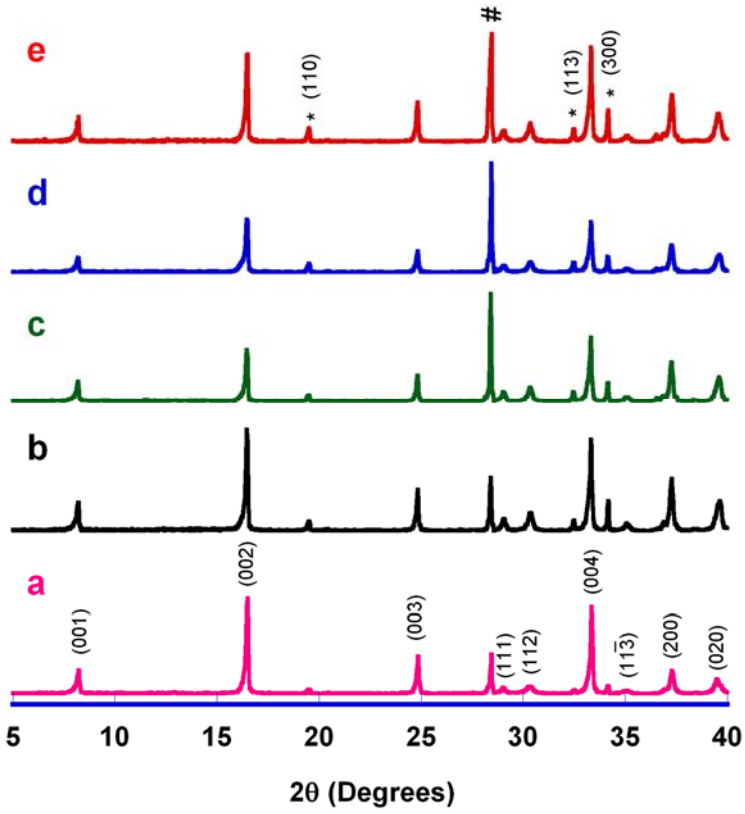
e
d
c
b
a
#
* (110)
* (113)
* (300)
(001)
(002)
(003)
(111)
(112)
(004)
(11$\bar{3}$)
(200)
(020)
5
10
15
20
25
30
35
40
2θ (Degrees)

Figure 2

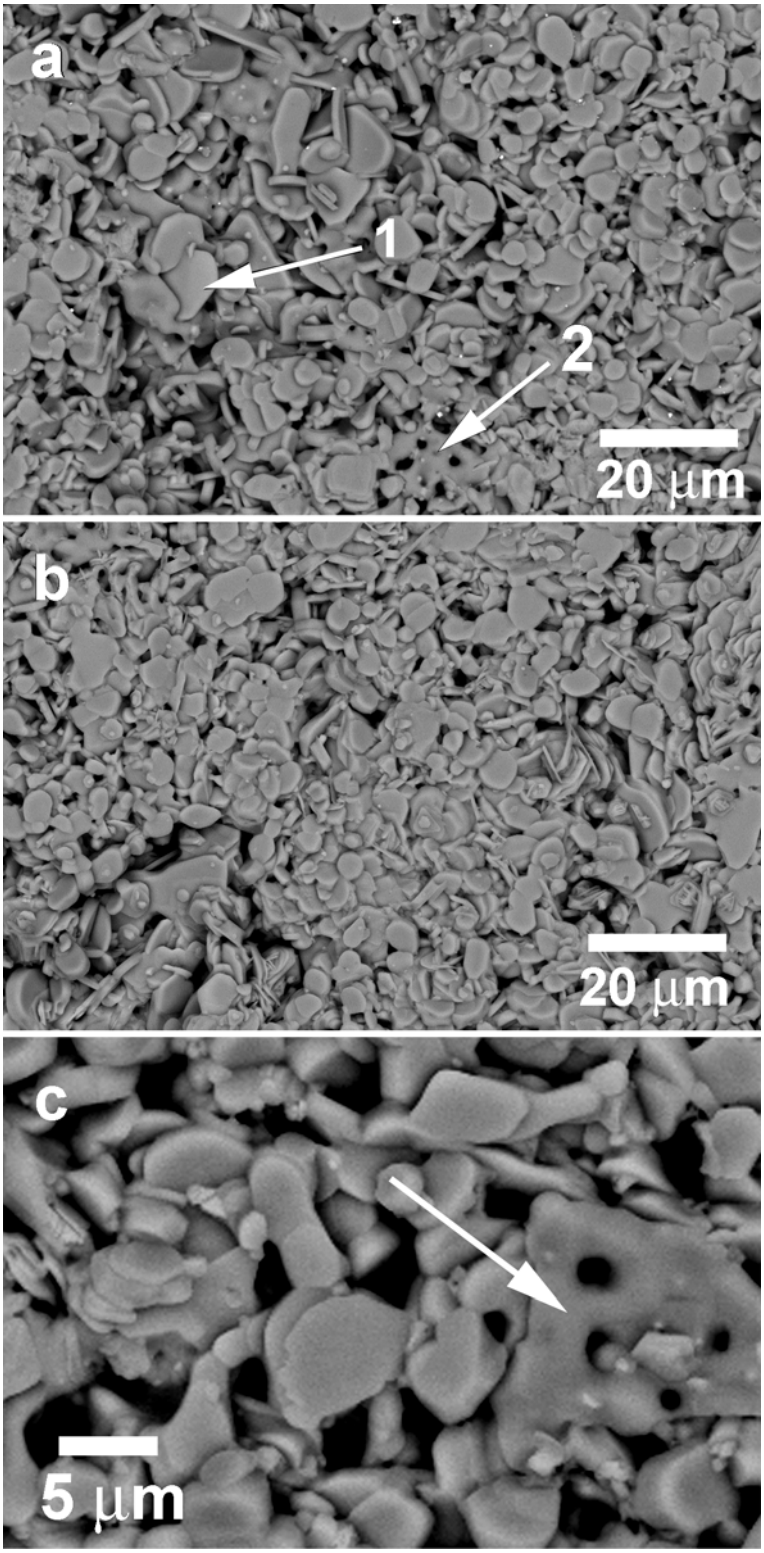

Figure 3

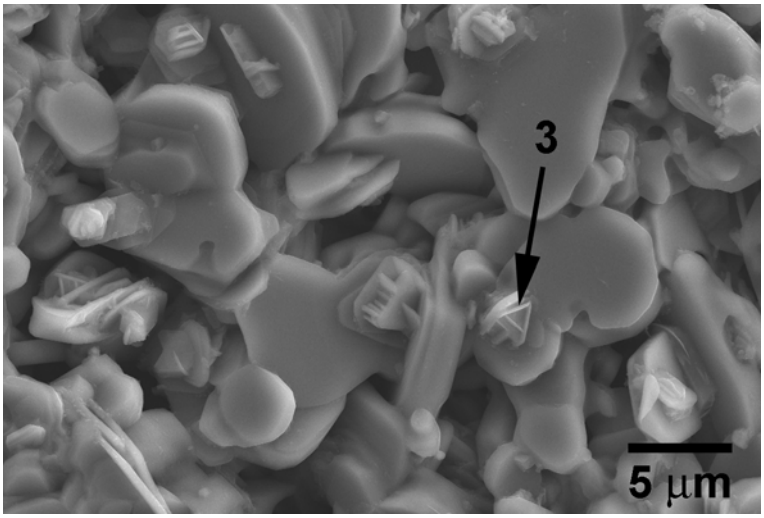

Figure 4

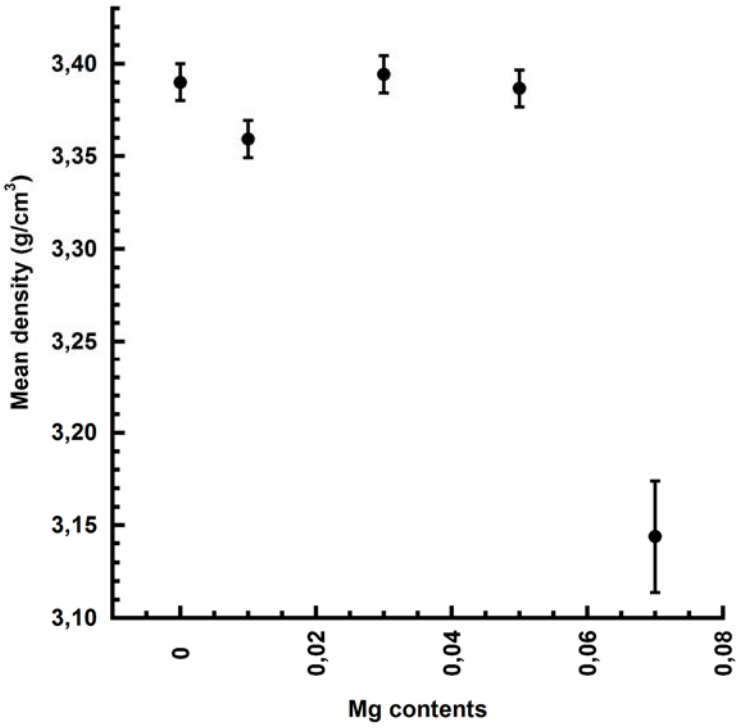
Mean density (g/cm^3)
3,40
3,35
3,30
3,25
3,20
3,15
3,10
0
0,02
0,04
0,06
0,08
Mg contents

Figure 5

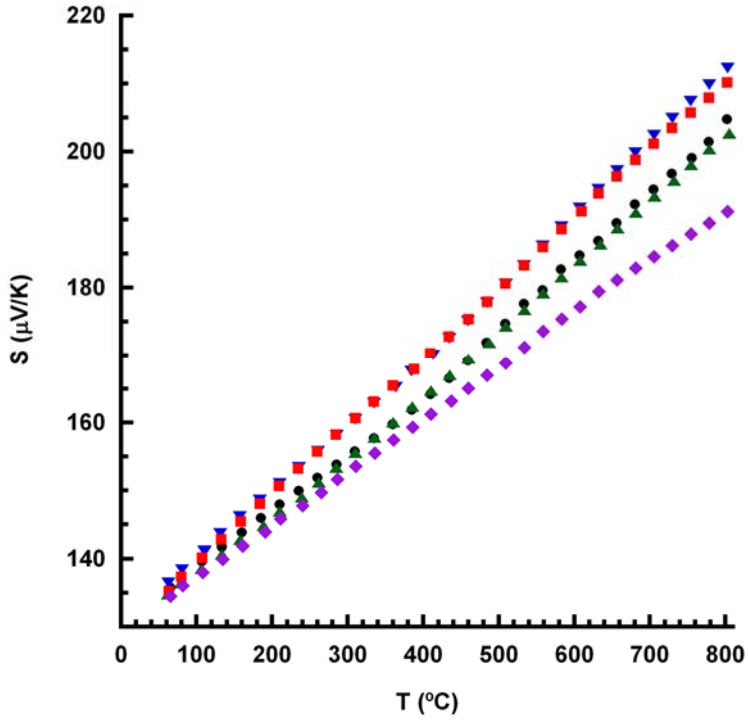

Figure 6

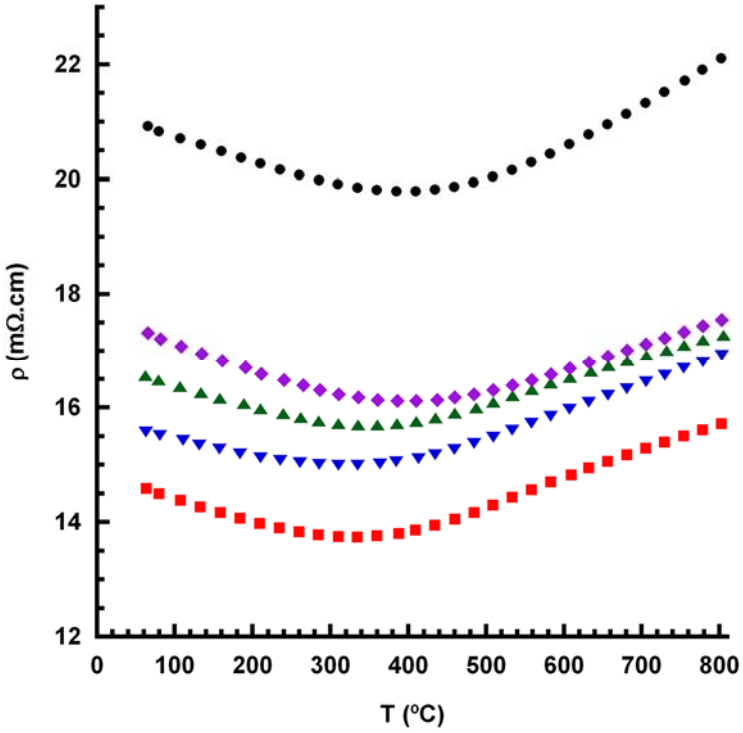

Figure 7

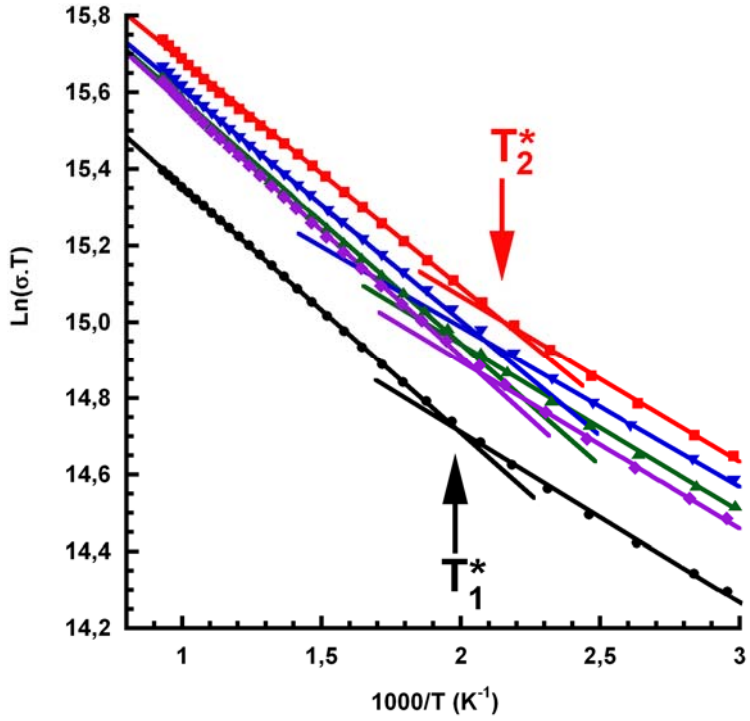

Figure 8

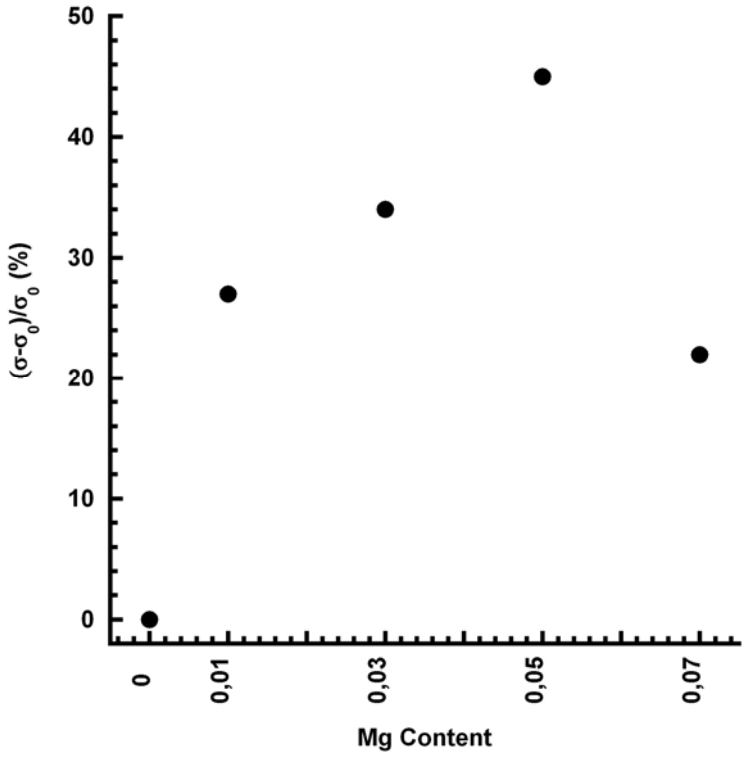

Figure 9

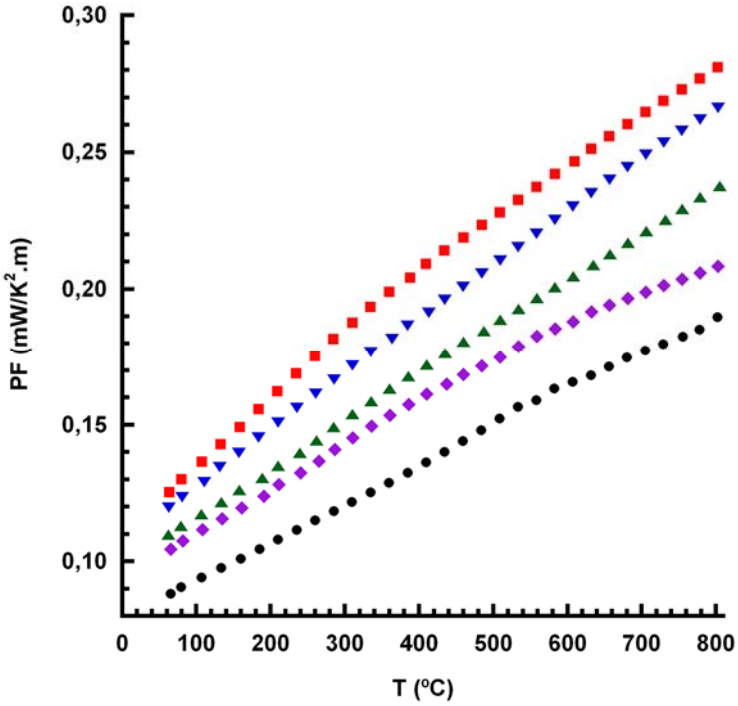
0,30
0,25
0,20
0,15
0,10
PF (mW/K².m)
0
100
200
300
400
500
600
700
800
T (ºC)